

Dalton Transactions

Accepted Manuscript



This is an *Accepted Manuscript*, which has been through the Royal Society of Chemistry peer review process and has been accepted for publication.

Accepted Manuscripts are published online shortly after acceptance, before technical editing, formatting and proof reading. Using this free service, authors can make their results available to the community, in citable form, before we publish the edited article. We will replace this *Accepted Manuscript* with the edited and formatted *Advance Article* as soon as it is available.

You can find more information about *Accepted Manuscripts* in the [Information for Authors](#).

Please note that technical editing may introduce minor changes to the text and/or graphics, which may alter content. The journal's standard [Terms & Conditions](#) and the [Ethical guidelines](#) still apply. In no event shall the Royal Society of Chemistry be held responsible for any errors or omissions in this *Accepted Manuscript* or any consequences arising from the use of any information it contains.

ARTICLE

Synthesis, structure, and peculiar green-emitting of NaBaBO₃:Ce³⁺ phosphor

Cite this: DOI: 10.1039/x0xx00000x

Ruijin Yu,^a Shengliang Zhong,^b Na Xue,^a Hongjuan Li,^a Hailong Ma^aReceived 00th January 2014,
Accepted 00th January 2014

DOI: 10.1039/x0xx00000x

www.rsc.org/

Polycrystalline samples of Ce³⁺-doped NaBaBO₃ (0.5-15 mol %) were prepared by the solid-phase synthesis. The phase formation was confirmed by X-ray powder diffraction (XRD) measurements and the structure refinement. The photoluminescence excitation and emission spectra, and decay curves were measured. The absolute luminescence quantum efficiency (QE) and the activation energy (ΔE) were reported. Under the excitation of near-UV light, Ce³⁺-doped NaBaBO₃ presents a green-emitting band centred at 505 nm from allowed inter-configurational 4f-5d transition. The maximum absolute QE of NaBaBO₃:Ce³⁺ was measured to be 58 % excited at 395 nm light at 300 K. The thermal stability of the green luminescence was evaluated by the luminescence decays as a function of temperature. The phosphor shows an excellent thermal stability on temperature quenching effects. Compared with the reported Ce³⁺-doped alkali metal and alkaline earth orthoborates with general formula *MNBO*₃ with only blue luminescence, the peculiarity of NaBaBO₃:Ce³⁺ is the green-emitting and a high doping concentration in the lattices. The results were discussed on the relationship between the structure and the luminescence properties.

Introduction

Rare-earth ions (RE) doped compounds have been widely investigated for the applications in luminescence performance and displays such as plasma display devices (PDP), field emission displays (FED), cathode ray tubes (CRT), electroluminescent displays (EL), laser generation, and white light-emitting diodes (WLEDs).¹⁻¹⁰ Fluorescence properties of RE ions strongly depend on the crystallographic environment in a host lattice. In the past decades, much research interest has been focused on the synthesis and characterization of inorganic borates for the exploration of nonlinear optical and luminescence materials.^{11,12}

It is well known that boron atom can be coordinated by oxygen atoms to form a variety of atomic groups. This is a dominant factor for the optical properties of borates.¹³ Borate phosphors have great potential in LED application, due to their low synthesizing temperature, various structures, and good chemical and physical stability. Recently, phosphors based on alkali (M) and alkaline earth (N) orthoborates with general formula *MNBO*₃ have been widely reported on the potential application as new materials in solid state lighting.^{14,15} The reports can be gathered in the following respects, (1) crystallographic studies such as LiCaBO₃,¹³ LiMgBO₃,¹⁶ NaCaBO₃,¹⁷ NaBaBO₃.¹⁸ (2) multiple-emission phosphors such as LiCaBO₃:Ce³⁺/Mn²⁺,¹⁹ LiSrBO₃:Sm³⁺,²⁰ NaCaBO₃:Ce³⁺/Tb³⁺/Mn²⁺,²¹ NaCaBO₃:Ce³⁺/²² NaCaBO₃:Ce³⁺/Mn²⁺/²³ NaCaBO₃:Sm³⁺,²⁴ NaSrBO₃:Ce³⁺,²⁵ NaSrBO₃:Tb³⁺,²⁶ NaSrBO₃:Sm³⁺,²⁷ NaSrBO₃:Ce³⁺/Mn²⁺,^{19,28} KCaBO₃:Er³⁺/Yb³⁺,²⁹ KCaBO₃:Dy³⁺/Eu³⁺,³⁰ and (3) Linear optics of such as LiSrBO₃ and LiBaBO₃.³¹

It can be seen from the reported references mentioned above that RE-doped *MNBO*₃ have been synthesized by different methods

to explore the luminescent properties for potential applications.¹³⁻³¹

The crystal structures of *MNBO*₃ are remarkably different depending on the different size of *M* and *N* ions. For example, LiMgBO₃ has monoclinic form (*C2/c*),³² LiCaBO₃ belongs to orthorhombic system (*Pbca*),¹³ while LiNBO₃ (*N*=Sr, Ba) compounds crystallize in the monoclinic space group *P2₁/n*.³¹ The planar BO₃ groups distribute differently in these compounds. The coordination manners of alkali metal and alkaline-earth metal are greatly diverse. Alkali metal and alkaline-earth metal are very active, and are easy to form various crystal structures with boric acid, which bring us a large field to find new luminescence materials.

In this work, Ce³⁺ ion was selected to be act as an activator in NaBaBO₃ host due to the fact that fluorescence of Ce³⁺ ions from allowed inter-configurational 4f-5d transition strongly depends on the crystallographic environment. At present, the luminescence of all the reported *MNBO*₃:Ce³⁺ are located in the blue region (420-450 nm), and the excitation wavelength locate in the UV region. Therefore, it is an interesting task to find an appropriate host of *MNBO*₃ in which Ce³⁺ ions can be effectively pumped by near UV light (400 nm) and emits longer wavelength luminescence such as green region. This is ideal situation for white light-emitting diodes (LEDs) fabricated with near-UV chips. In our experiments, NaBaBO₃ host was confirmed to be an appropriate host to accommodate Ce³⁺ ion and present green or yellowish-green luminescence with the excitation in the near UV region.

The samples were synthesized by the solid state reaction. The structure was investigated by powder X-ray powder diffraction (XRD) and refinements. The photoluminescence spectra and decay curves were measured. The thermal stability of the green luminescence was evaluated by the luminescence decays as a function of temperature. The absolute luminescence quantum efficiency (QE) and the activation energy (ΔE) were reported.

Experimental section

Polycrystalline powder NaBaBO_3 samples with different concentrations of Ce^{3+} (0.5-15 mol %) were prepared by three-step solid-phase synthesis. The starting materials were Na_2CO_3 , H_3BO_3 , BaCO_3 , and CeO_2 (Aldrich, 99.99%). Stoichiometric amount of raw materials were mixed homogeneously and placed in a corundum crucible. 5% excess of H_3BO_3 was added in the raw materials for the compensation of evaporation at high temperature. Firstly, the stoichiometric mixture was slowly heated up to 350-450 °C in 7 h and kept at this temperature for 5 h to decompose H_3BO_3 by removing H_2O . Secondly, the obtained powder was finely grinded again and then heated up to 650-700 °C for 5 h in air in order to make get a high mixing uniformity of the particles for an easy reaction with each other. Finally, the materials were thoroughly mixed by grinding in an agate mortar, then heated at 800-850 °C for 2.5-5 h under 5:95 (H_2/N_2) atmosphere to reduce to Ce^{3+} activators.

The final products were monitored by powder X-ray diffraction analysis, which was collected on a Rigaku D/Max diffractometer operating at 40 kV, 30 mA with Bragg-Brentano geometry using $\text{Cu-K}\alpha$ radiation ($\lambda=1.5405 \text{ \AA}$). Structural refinements were made using the GSAS (general structure analysis system) program.³³ Scanning electron micrograph (SEM) images and electron dispersive X-ray (EDX) were obtained using a JEOL, JSM-6360 LA instrument. Photoluminescence spectra were recorded on a Perkin-Elmer LS-50B luminescence spectrometer with Monk-Gillieson type monochrometers and a xenon discharge lamp was used as excitation source. For the measurements of luminescence decay curves, the samples were excited by a pulsed Nd:YAG laser at 355 nm (Spectron Laser System SL802G). The luminescence was dispersed by the 75 cm monochromator (ActonResearch Corp. Pro-750) and multiplied by the PMT (Hamamatsu R928). The data was displayed and recorded with the LeCloy 9301 digital storage oscilloscope.

Results and discussions

The crystal phase formation

Table 1 Refined crystallographic parameters of Ce^{3+} -doped NaBaBO_3

formula	NaBaBO_3
radiation	Cu Ka
2θ range (degree)	10-70
symmetry	monoclinic
space group#	C2/m
$a/\text{\AA}$	9.5763(11)
$b/\text{\AA}$	5.5683(7)
$c/\text{\AA}$	6.1892(7)
$\alpha/^\circ$	90
$\beta/^\circ$	98.885(7)
$\gamma/^\circ$	90
Z	4
R_p	1.8463
R_{wp}	0.3094
χ^2	21.04
$V/\text{\AA}^3$	326.07(10)

The representative XRD structural refinements of $\text{NaBaBO}_3:\text{Ce}^{3+}$ were carried out using GSAS program.³³ Fig. 1 plots experimental, calculated, and different results from the refinements of $\text{NaBaBO}_3:0.05\text{Ce}^{3+}$. The refined parameters are listed in Table 1. The results indicate that the Ce^{3+} ions were completely incorporated

into each the host lattices without making significant changes to the crystal structure. The consistent result indicated that the single phase NaBaBO_3 powders were obtained in this solid state reaction. It is difficult for Ce^{3+} ions to substitute with Na^+ (1.02 Å, CN = 6) or B^{3+} (0.39 Å, CN = 3) in the NaBaBO_3 lattices. The ionic radius ($r = 1.196 \text{ \AA}$, CN = 9) of Ce^{3+} ion is close to that of Ba^{2+} (1.47 Å, CN = 9). Hence, it was suggested that the Ba^{2+} sites are replaced by Ce^{3+} ions in the lattice.

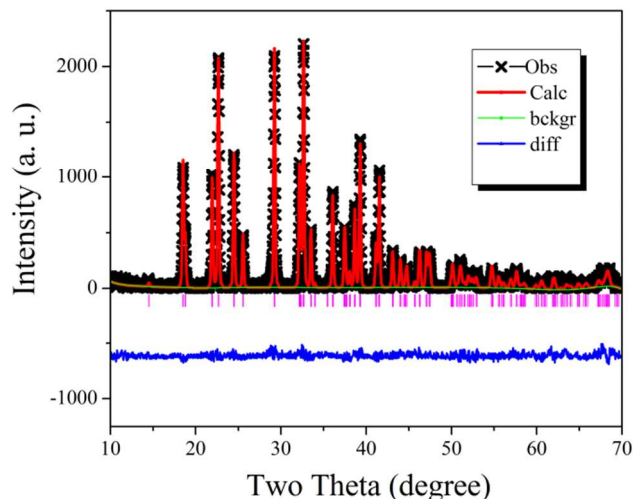


Fig.1 Representative experimental (crossed) and calculated (red solid line) X-ray diffraction profiles of $\text{NaBaBO}_3:0.05\text{Ce}^{3+}$. The difference profile is located at the bottom of the figure.

Table 2 Refined atomic coordinate parameters of Ce^{3+} -doped NaBaBO_3 .

Atom	Wyck	Site	x/a	y/b	z/c	$U[\text{\AA}^2]$
Ba1	4i	m	0.6661(5)	0	0.7401	0.0768
Na1	2a	2/m	0	0	0	0.218
Na2	2c	2/m	0	0	1/2	0.0621
O1	4i	m	0.7983(3)	0	0.193	0.094
O2	8j	1	0.5845(2)	0.224	0.2634	0.0311
B1	4i	m	0.6503(3)	0	0.305	-0.090

The refinement parameters of the atomic coordinates of $\text{NaBaBO}_3:\text{Ce}^{3+}$ are given in Table 2. The structure sketch map of Ce^{3+} -doped NaBaBO_3 is shown in Fig. 2, which was modeled using the Diamond Crystal and Molecular Structure Visualization software on the basis of the atomic coordinate's data from XRD refinements in Table 2. This is in agreement with Tu et al's report.³⁵ NaBaBO_3 crystallizes in the monoclinic system, space group C2/m. The structure contains a triangular BO_3 group, a BaO_9 polyhedron and two crystallographically distinct distorted NaO_6 octahedra.

In sodium alkaline earth metal (N) based orthoborates NaNBO_3 , an interesting case is that no matter what coordination manners the Na atoms take, the Na-centered polyhedra will form chains along the c-axis by edges and faces in those orthoborates.^{34,35} This is a discerning feature of the structure is the presence of one-dimensional chains of face-shared NaO_6 octahedra that extend along the c axis. The octahedra are linked through the planar BO_3 triangles to form a framework, whose cavities are occupied by large Ba^{2+} cations.^{34,35} The octahedral share face and edge with the BaO_9 groups and vertices with the BO_3 planes as shown in Fig. 2 (b).

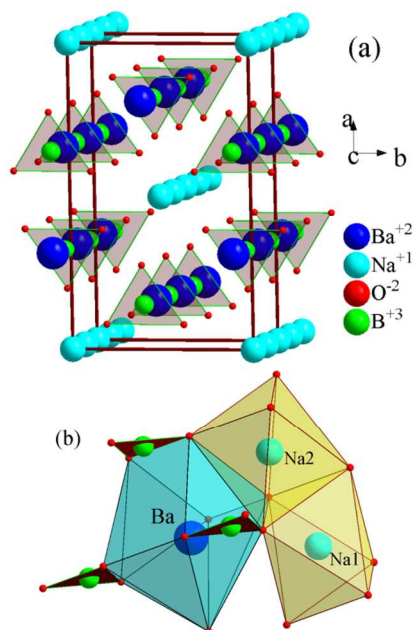


Fig. 2 (a) schematic views of the NaBaBO_3 structure along the c -direction; (b) the structural diagram with Ba and Na atoms' sites.

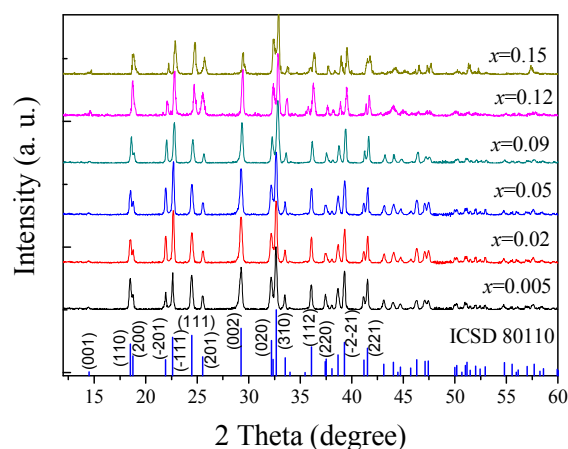


Fig. 3 XRD patterns of $\text{NaBaBO}_3:\text{xCe}^{3+}$ phosphors ($x=0.005$ - 0.15). The experimental patterns were compared with the corresponding standard cards ICSD 80110.

The phase purity of the as-prepared Ce^{3+} -doped NaBaBO_3 phosphors with different doping concentrations were also checked by XRD measurements. As seen in Fig. 3, XRD patterns of all the samples show similar profiles except the small difference for the intensity of some XRD peaks. For example, the (001) peak can be noticed for $x=0.15$ and 0.12 which is very weak for $x=0.02$, 0.05 , and 0.09 . This could be due to the difference of crystalline habit with the different Ce^{3+} doping, for example, the (001) face could be well developed with high Ce^{3+} doping in the NaBaBO_3 lattices. All the diffraction peaks of these samples are in good agreement with the ICSD standard pattern, indicating that the obtained NaBaBO_3 samples are single phase. No characteristic peaks from any impurities were detected, indicating that the Ce^{3+} doping does not cause any detectable change in the host structure.

To confirm the crystalline morphology of the polycrystals, the SEM images were investigated. Fig. 4 shows the typical scanning electron microscopy images of $\text{NaBaBO}_3:\text{xCe}^{3+}$ with $x=0$ (a), $x=0.05$ (b), $x=0.12$ (c) and $x=0.15$ (d) phosphors sintered at 800°C . The

powders are generally consisted of spheroidal particles with the uniform morphology in each sample. It is seen that the particles have a good quality of crystalline. This indicates that the solid state reactions of the mixtures took place well. It can be found that the undoped sample ($x=0$) presents a larger particle size ranging from 3 to $5\ \mu\text{m}$ than the Ce^{3+} -doped samples. With the increase of Ce^{3+} doping (as shown Fig. 4 b, c and d), the particle size becomes small and the distribution becomes narrow as compared to the undoped sample. The average size estimated in $\text{NaBaBO}_3:0.15\text{Ce}^{3+}$ phosphor is a diameter of 1 - $3\ \mu\text{m}$.

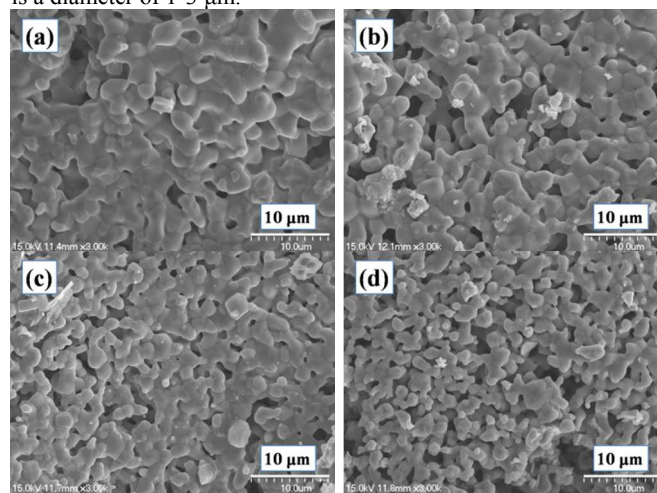


Fig. 4 Typical SEM images of $\text{NaBaBO}_3:\text{xCe}^{3+}$ phosphors with $x=0$ (a), $x=0.05$ (b), $x=0.12$ (c), $x=0.15$ (d).

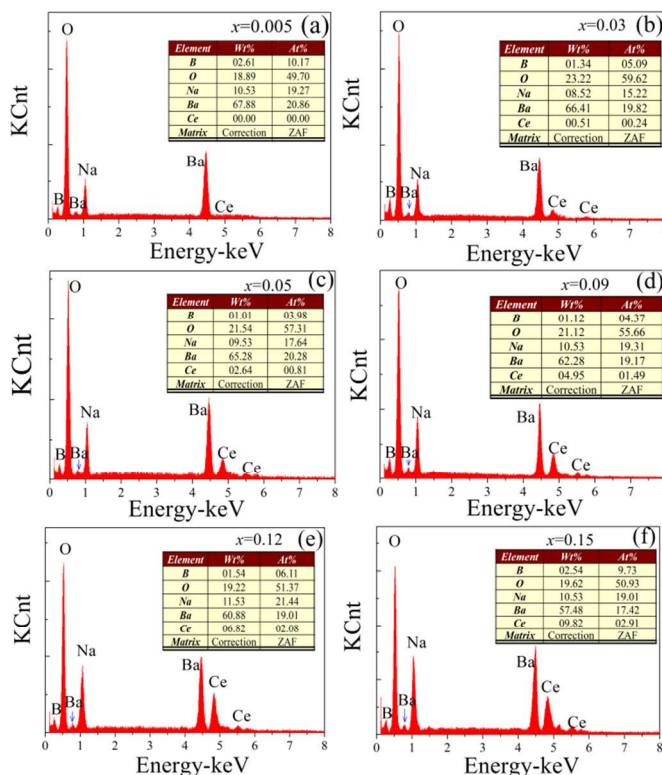


Fig. 5 Typical EDX spectra of $\text{NaBaBO}_3:\text{xCe}^{3+}$ with $x=0.005$ (a), $x=0.03$ (b), $x=0.05$ (c), $x=0.09$ (d), $x=0.12$ (e), and $x=0.15$ (f). Inset shows the quantitative ratio of the elements calculated from EDX data.

The energy-dispersive X-ray (EDX) spectroscopy was used to examine the elemental compositions of $\text{NaBaBO}_3:\text{xCe}^{3+}$. The representative EDX spectra of $\text{NaBaBO}_3:\text{xCe}^{3+}$ with $x=0.005$ (a),

$x=0.03$ (b), $x=0.05$ (c), $x=0.09$ (d), $x=0.12$ (e), and $x=0.15$ (f) are shown in Fig. 5. Several specific lines on EDX spectra show the signals of O, B, Ba, Na, and Ce elements in the as-prepared samples. The quantificational ratio for the elements is listed inset in Fig. 5. In $\text{NaBaBO}_3:0.005\text{Ce}^{3+}$ phosphor Ce^{3+} concentration in the sample is under the detectable limitation. The amounts of Ce^{3+} ions obtained by EDX analysis in $\text{NaBaBO}_3:x\text{Ce}^{3+}$ increases with the enhancement of Ce^{3+} doping from $x=0.05$ to 0.15. It was observed that the measured calculated values for B and Ce are lower than those in the precursors, but it can confirm the Ce^{3+} doping in the host lattices. No Ce^{4+} ions were detected in all the samples.

Photoluminescence properties

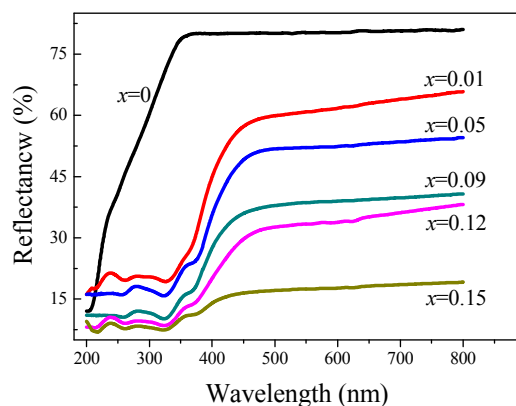


Fig. 6 Diffuse reflectance spectra of $\text{NaBaBO}_3:x\text{Ce}^{3+}$ ($x=0, 0.01, 0.05, 0.09, 0.12, 0.15$).

The comparison of the reflectance spectra between NaBaBO_3 host and $\text{NaBaBO}_3:x\text{Ce}^{3+}$ ($x=0.01, 0.05, 0.09, 0.12, 0.15$) phosphors is shown in Fig. 6. The diffuse reflection spectrum of the host has a status of high reflection in the wavelength ranging from 350 to 800 nm and decreasing intensity from 350 to 200 nm. The abrupt drop in the reflection spectrum can be attributed to the host absorption, i.e. valence-to-conduction band transition of the NaBaBO_3 host. From the reflection spectrum, a roughly estimated optical band-gap of NaBaBO_3 is about 6.2 eV. There is the obvious difference in the spectral profiles of Ce-doped NaBaBO_3 compared to that of the host. The strong broad absorption appeared in the 200–450 nm wavelength range, which was attributed to the $4f$ - $5d$ electronic transition absorption of the Ce^{3+} ions. The absorption intensities increase gradually with increasing Ce^{3+} concentration. In the meantime, the absorption edge of Ce^{3+} -doped samples shifts to longer wavelength, i.e., low energy, varying from $x=0.01$ to 0.15. In order to support observations of diffuse reflection spectrum, the PL and PLE spectra of the $\text{NaBaBO}_3:x\text{Ce}^{3+}$ phosphors were investigated.

Fig. 7 shows the typical luminescence spectrum in 0.5 mol% Ce^{3+} -doped NaBaBO_3 phosphor under excitation of 395 nm. It indicates that the as-synthesized $\text{NaBaBO}_3:0.5\% \text{Ce}^{3+}$ phosphor exhibits a green-emitting band peaking at 505 nm, which corresponds to the Ce^{3+} $5d \rightarrow 4f$ transition. It is well known that Ce^{3+} ion spectrum has a double emission band corresponding to the splitting between the ${}^2F_{5/2}$ and the ${}^2F_{7/2}$ states due to the spin-orbit coupling. This emission can be deconvoluted into two Gaussian bands corresponding to the $5d \rightarrow {}^2F_{5/2}$ and $5d \rightarrow {}^2F_{7/2}$ transitions as shown inset Fig. 7. The emission spectrum can be decomposed into two Gaussian components Xc:20,280 cm^{-1} (493 nm) and Xc2: 18,100 cm^{-1} (552 nm), which are corresponding to the transitions of $5d \rightarrow {}^2F_{5/2}$ and $5d \rightarrow {}^2F_{7/2}$, respectively (Inset Fig. 7). The energy

difference between these two bands is 2180 cm^{-1} . This value is consistent with the difference of about 2,000 cm^{-1} between the two ground states ${}^2F_{5/2}$ and ${}^2F_{7/2}$ of Ce^{3+} .³⁶ This implies that there is only one type of Ce^{3+} luminescence site in NaBaBO_3 lattice, which is consistent with the fact only a single crystallographic Ba site available for Ce^{3+} doping. This is in agreement with the reported structure data.

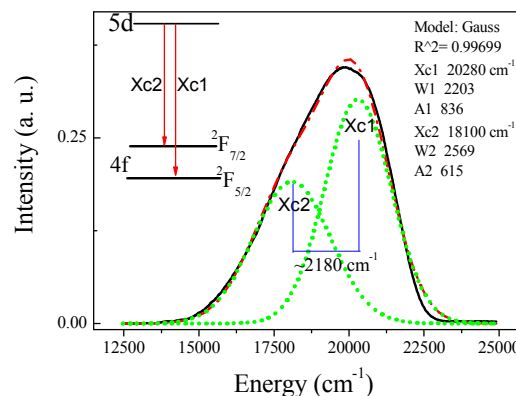


Fig. 7 the emission spectra of $\text{NaBaBO}_3:0.005\text{Ce}^{3+}$ under excitation of 395 nm; the Gaussian fit into two components Xc: 20,280 cm^{-1} (493 nm) and Xc2: 18,100 cm^{-1} (552 nm) for emission band. Inset is the schematic diagram of Ce^{3+} ions with $4f$ - $5d$ absorption and two emission bands.

At present, the luminescence of all the Ce^{3+} -doped MNBO_3 phosphors have been reported to present blue luminescence, for example, $\text{NaSrBO}_3:0.01\text{Ce}^{3+}$ (426 nm in Ref²⁵, 430 nm in Ref²⁸), $\text{NaCaBO}_3:0.01\text{Ce}^{3+}$ (427 nm,²¹ 421 nm²², 400 nm²³), $\text{LiCaBO}_3:0.01\text{Ce}^{3+}$ (420 nm)¹⁹. It can be noted that the emission wavelength of Ce^{3+} -doped NaBaBO_3 is much longer than any of the reported values. This can be explained by the influence of the crystal structure in NaBaBO_3 lattices. As shown in Fig. 2 (b), the BaO_9 polyhedral is greatly deformed because it is connected with NaO_6 by sharing face and edge in the lattices. This may further suppress the lowest excited (the emitting state) state of Ce^{3+} ions when compared to the other MNBO_3 borates. This leads to the emission maximum shifted to longer wavelengths.

The excitation spectrum of $\text{NaBaBO}_3:\text{Ce}^{3+}$ phosphor is shown in Fig. 8 by monitoring with an emission wavelength of 505 nm. The PLE spectrum shows a broad band between 250 and 430 nm with the maximum wavelength at 395 nm, which can be attributed to $4f$ - $5d$ transition of Ce^{3+} ions. Inset show the normalized spectra for $\text{NaBaBO}_3:\text{Ce}^{3+}$ phosphor. The spectra show two peaks at 338 nm and 395 nm. With increasing the doping of Ce^{3+} concentration, the shoulder at high energy site (338 nm) decreases its intensity. And no obvious shift can be observed at different doping concentrations. It suggests that the $\text{NaBaBO}_3:\text{Ce}^{3+}$ phosphor can be effectively excited by near UV chips (360–400 nm). This is necessary for the potential application in the white LEDs fabricated with near-UV chips. This is very different from the reported phosphors of Ce^{3+} -doped MNBO_3 (<350 nm), which have only favorite excitation in the UV wavelength band. The observed Stokes shift of approximately 5510 cm^{-1} , is in the normally reported value for Ce^{3+} doped phosphors in the range 3200–7200 cm^{-1} .³⁷

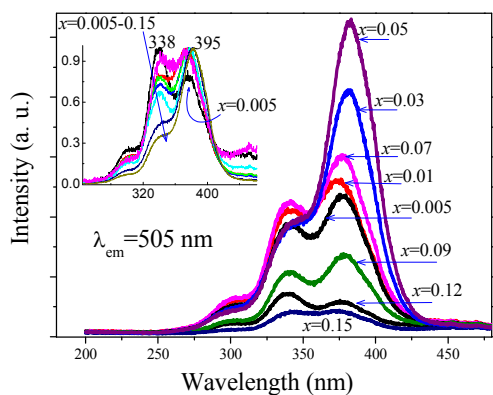


Fig. 8 Excitation spectra of $\text{NaBaBO}_3:\text{xCe}^{3+}$ ($x=0.005, 0.01, 0.03, 0.05, 0.07, 0.09, 0.12, 0.15$) at 300 K. inset is the normalized spectra to compare the excitation profile.

Luminescence quenching on doping concentration

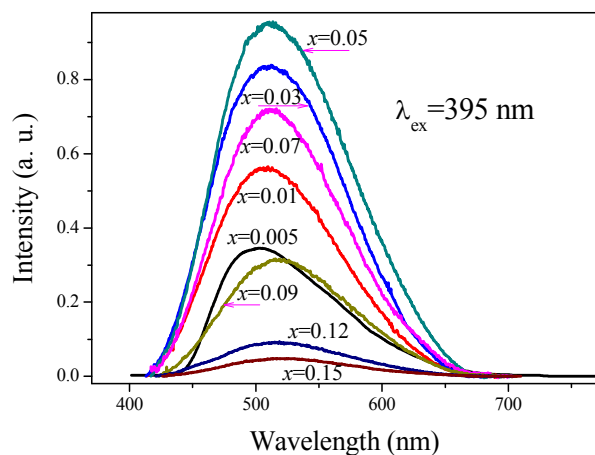


Fig. 9 Emission spectra of $\text{NaBaBO}_3:\text{xCe}^{3+}$ ($x=0.005, 0.01, 0.03, 0.05, 0.07, 0.09, 0.12, 0.15$) under excitation of 395 nm.

Fig. 9 shows the emission spectra of a series of $\text{NaBaBO}_3:\text{xCe}^{3+}$ phosphors with different concentrations under excitation of near-UV light at 395 nm. It exhibited a broad-band green emission peak covering the spectral region from 400 to 650 nm centered at 505 nm.

Fig. 10 shows the dependence of integrated intensity on the Ce^{3+} -doping concentration in NaBaBO_3 . It can be also found that the emission intensity tends to enhance with an increase in the Ce^{3+} concentration and it reaches the maximum of intensity at $x=0.05$. Consequently, the concentration quenching occurs as the contents of Ce^{3+} are beyond 0.05, namely, the emission intensity declines dramatically as the content of Ce^{3+} exceeds 0.05. This shows that the optimum doping for Ce^{3+} ions in NaBaBO_3 is 5 mol %. It can be noted that the maximum doping for Ce^{3+} ions in NaBaBO_3 can reach as high as 15 mol %, and the sample keeps the pure crystal phase formation as shown in Fig. 3. This indicates that NaBaBO_3 host has strong capability to adopt high concentration of trivalent rare-earth ions.

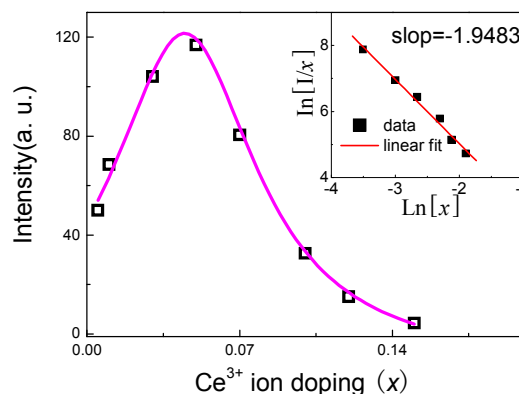


Fig. 10 The dependence of intensity of $\text{NaBaBO}_3:\text{xCe}^{3+}$ ($x=0.005, 0.01, 0.03, 0.05, 0.07, 0.09, 0.12, 0.15$) on the Ce^{3+} -doping concentration. Inset is the fitting curve of $\ln(I/x)$ versus $\ln(x)$ in $\text{NaBaBO}_3:\text{xCe}^{3+}$ ($x=0.005-0.15$) phosphors

In order to estimate the critical energy transfer distance (R_c) between the activators in the host, the following equation can be used as there is only one crystallographic Ba^{2+} site in the NaBaBO_3 lattice. Consequently, the critical energy transfer distances between Ce^{3+} ions can be estimated by the equation as:

$$R_c = 2\left(\frac{3V}{4\pi x_c Z}\right)^{\frac{1}{3}} \quad (1)$$

here x_c is the critical concentration, Z is the number of cation site in unit cell, and V is the volume of unit cell. In this phosphor, $V=326 \text{ \AA}^3$, $Z=4$ and the critical doping concentrations of Ce^{3+} in the host was found to be 0.05. Thus, R_c of Ce^{3+} was estimated to be 14.6 \AA .

Since the luminescence mechanism is $4f \rightarrow 5d$ allowed electric-dipole transition, the process of energy transfer should occur as the electric multipolar interactions process according to Dexter theory.³⁸ If the energy transfer occurs between the same sorts of activators, then the intensity of multipolar interaction can be determined from the change of the emission intensity from the emitting level which has a multipolar interaction. The emission intensity (I) per one activator ion follows the equation:³⁹

$$\frac{I}{x} = K[1 + \beta(x)^\theta]^{-1} \quad (2)$$

where, x is the activator concentration; K and β are constants for the same excitation condition in a given host crystal, and θ is an indication of electric multipolar character. When the θ value is 6, 8, 10, the quenching process is dipole-dipole, dipole-quadrupole, quadrupole-quadrupole, respectively. When x is larger than the critical quenching concentration x_c , Eq. (2) can approximately be expressed by Eq. (3) for $\beta(x)^{\theta/3} \gg 1$, where K' is a constant.³⁹

$$\frac{I}{x} = K' / \beta(x)^\theta \quad (3)$$

In order to get the quenching parameter value of θ , the dependence of $\log(I/x)$ on $\log(x)$ can be plotted, and it results in a straight line with a slope equal to $-\theta/3$. Inset Fig. 10 plots the fit of $\ln(I/x)$ versus $\ln(x)$ in $\text{NaBaBO}_3:\text{xCe}^{3+}$ phosphors. It is a linear with a slope of -1.9483 . The value of θ can be calculated as 5.85, which is approximately equal to 6. It indicates that the dipole-dipole interaction is dominated concentration quenching mechanism of the Ce^{3+} emission center in the $\text{NaBaBO}_3:\text{xCe}^{3+}$ phosphor.

Table 3 QE values of Ce³⁺-doped NaBaBO₃ and the results from references.

Sample	Excitation (nm)	Emission n (nm)	QE (%)	Note
NaBaBO ₃ :0.05Ce ³⁺	395	505	58	This work
BAM:Eu ²⁺	400	450	41	Ref. 40
BAM:Eu ²⁺	365	450	98.4	Ref. 25
YAG:Ce (bulk)	430	560	61.0	Ref. 41
CREE				
YAG:Ce (nano)	430	560	54.0	Ref. 41
YAG:Ce ³⁺ (nano)	430	525	45	Ref. 42
YAG:Ce ³⁺ (powder)	465	530	38.4	Ref. 43
(Y _{0.95} Eu _{0.05}) ₂ O ₃	394	611	3.0	Ref. 43
Y ₂ O ₂ S:Eu ³⁺	317	611	35	Ref. 44

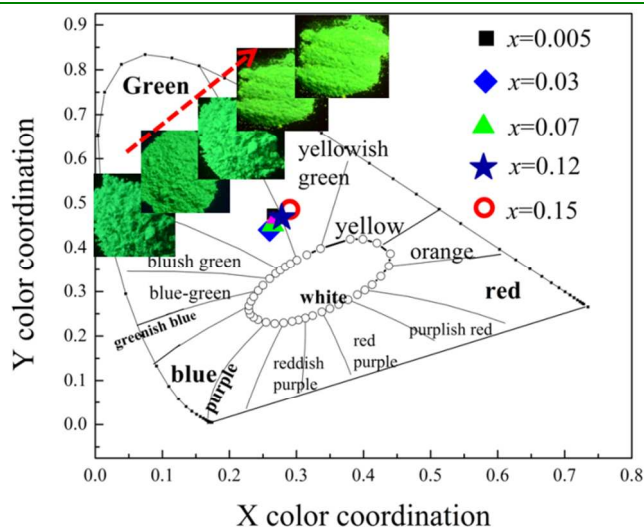


Fig. 11 CIE chromaticity coordinates of the selected NaBaBO₃:xCe³⁺ (x=0.005, 0.03, 0.07, 0.12, 0.15) phosphors. Inset is the images of the phosphors excited at 365 nm lamp.

The QE value of NaBaBO₃:0.05Ce³⁺ measured (excitation 395 nm) at room temperature is 58 %. The result is compared with the reported phosphors in Table 3, for example, the commercial blue phosphor BaMgAl₁₀O₁₇:Eu²⁺ (BAM:Eu²⁺), green Y₃Al₅O₁₂:Ce³⁺ (YAG:Ce³⁺) and red Y₂O₂S:Eu³⁺. QE for NaBaBO₃:Ce³⁺ is comparable with YAG:Ce³⁺ and BAM:Eu²⁺, and is better than Eu³⁺-doped Y₂O₃ and Y₂O₂S. Usually QE usually of a phosphor depends on many influences, for example, excitation wavelength, synthesis conditions, dispersion ability and particle sizes, etc. For example, it has been confirmed that the luminescence of the YAG:Ce³⁺ are strongly dependent on the particle size and the redox reaction of cerium.⁴¹ The QE of NaBaBO₃:xCe³⁺ could be further enhanced by further improving the synthesis conditions (such as control the use of the flux) to get a high crystallization of the phosphors.

All the samples show green color under the excitation of near UV light as shown by the photos inset Fig. 11, which could also be confirmed by the CIE (Commission International de l'Eclairage, 1931) coordinates calculated from emission spectra. The CIE chromaticity coordinates of NaBaBO₃:xCe³⁺ (x=0.005, 0.03, 0.07, 0.12, 0.15) are shown in Fig. 11, which are in the green color region. With the increase Ce³⁺ doping, the color of NaBaBO₃:xCe³⁺ has a small change from the green to yellowish green region.

Luminescence decay and thermal stability on temperature

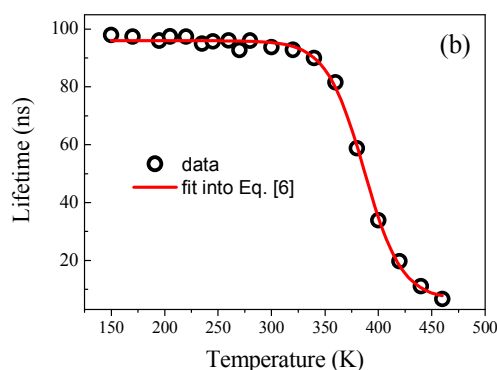
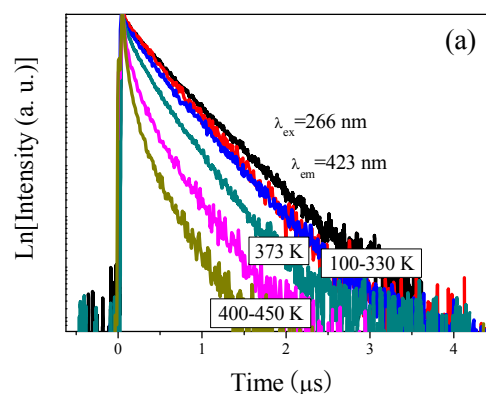


Fig. 12 (a): Temperature-dependent decay curves of NaBaBO₃:xCe³⁺ phosphor under the excitation of 355 nm of a pulsed Nd:YAG laser; (b): The temperature-dependent luminescence lifetimes, Inset shows the temperature dependent lifetimes of the Ce³⁺ emission fitted into the Eq. [6].

In general, the temperature dependence of phosphors used in phosphor-conversion white LEDs is important because it has great influence on the light output and color rendering index. The thermal stability of Ce³⁺ phosphor was evaluated by the temperature-dependent luminescence decay process. Fig. 12 (a) shows the luminescence decay curves of Ce³⁺ phosphor at different temperatures. The curves at 100-330 K keep the single exponential behavior, which can be fitted into an approximate function as

$$I = I_0 + A \exp(-t/\tau) \quad (4)$$

where I_0 is the initial emission intensity for $t=0$ and τ is the lifetime. At a high temperature above 330 K, the luminescence decay of NaBaBO₃:Ce³⁺ displays a non-exponential curve, which can be fitted to the effective lifetime defined as:

$$\tau_{average} = \frac{\int_0^{\infty} I(t)tdt}{\int_0^{\infty} I(t)dt} \quad (5)$$

here $I(t)$ represents the luminescence intensity at a time t after the cutoff of the excitation light. The luminescence lifetimes of the Ce³⁺ ions are calculated as a function of temperature and displayed in Fig 12 (b). The decay time keeps near a constant (around 90 ns) up to 330 K. The decay time in Ce³⁺ drops at higher temperature from 330 K, presenting a typical temperature quenching behavior. The thermal activation energy (ΔE), the energy required to raise the electron from the relaxed excited level into the lattice conduction band, was determined by measuring the temperature dependence on the Ce³⁺

emission lifetime. The drawn line in the figure is fitted to the equation as:

$$\tau(T) = \frac{\tau_r}{1 + [\tau_r / \tau_{nr}] \exp(-\Delta E / kT)} \quad (6)$$

where k is the Boltzmann constant, τ_r and τ_{nr} are radiative and nonradiative decay times. The thermal activation energy for thermal quenching (ΔE) is fitted to be 0.283 eV. This value is much higher than that of NaSrBO₃:Ce³⁺ phosphor (0.0798 eV)²⁵. Considering that the operation temperature for the normal LEDs lamp should be 100–150 °C, it could be suggested NaBaBO₃:Ce³⁺ exhibit good thermal stability for its potential application in w-LEDs.

Conclusions

Ce³⁺ (0.5–15 mol %) doped NaBaBO₃ polycrystalline samples were prepared by solid-phase synthesis. The structure and luminescence characteristic were investigated. Under excitation of near UV light, NaBaBO₃:Ce³⁺ shows bright green color with maximum wavelength peaking at 505 nm from the Ce³⁺ 5d→4f transition. This is different from the color in the reported phosphors based on Ce³⁺-doped alkali (M) and alkaline earth (N) orthoborates with general formula MNBO₃, which has only blue emission. The occupation of Ce³⁺ ions on the deformed BaO₆ polyhedral in NaBaBO₃ lattices produce stronger crystal field and suppress the lowest excited (the emitting state) of Ce³⁺ ions, leading to the red-shift in emission wavelengths. The optimum doping for Ce³⁺ ions in NaBaBO₃ is 5 mol %. The absolute QE of NaBaBO₃:Ce³⁺ was measured to be 58 % at the excitation of 395 nm light. NaBaBO₃:Ce³⁺ has an excellent thermal stability on the temperature quenching with a high activation energy of $\Delta E=0.283$ eV. Due to the efficient excitation in the near UV region (250 and 430 nm), high luminescence efficiency, and good thermal stability, NaBaBO₃:Ce³⁺ phosphor could be a potential green-emitting phosphor for lighting and display such as white LEDs fabricated with near-UV chips.

Acknowledgements

This work was supported by the National Natural Science Foundations of China (Grant No. 21201141), the Chinese Universities Scientific Fund (Grant No. QN2011119), and the Open Foundation of Key Laboratory of Photoelectric Technology and Functional Materials (Culture Base) in Shaanxi Province (ZS12020). This work was also supported by the National Natural Science Foundation of China (Nos. 21201089, 21261010), Jiangxi Provincial Education Department (No. KJLD13021).

Notes and references

^a College of Science, Northwest A&F University, Yangling, Shaanxi 712100, P R China, E-mail address: yuruijin@nwsuaf.edu.cn (Ruijin Yu)

^b College of Chemistry and Chemical Engineering, Jiangxi Normal University, 99 Ziyang Road, Nanchang 330022, Jiangxi, China

- 1 D. W. Wen and J. X. Shi, *Dalton Trans.*, 2013, 42, 16621.
- 2 Z. G. Xia and W. W. Wu, *Dalton Trans.*, 2013, 42, 12989.
- 3 W. Z. Lv, W. Lü, N. Guo, Y. C. Jia, Q. Zhao, M. M. Jiao, B. Q. Shao and H. P. You, *Dalton Trans.*, 2013, 42, 13071.
- 4 R. Marin, M. Back, N. Mazzucco, F. Enrichi, R. Frattini, A. Benedetti and P. Riello, *Dalton Trans.*, 2013, 42, 16837.
- 5 J. Qiao, J. H. Zhang, X. Zhang, Z. D. Hao, Y. F. Liu and Y. S. Luo, *Dalton Trans.*, 2014, 43, 4146.
- 6 X. M. Wang, X. Zhang, S. Ye and X. P. Jing, *Dalton Trans.*, 2013, 42, 5167.
- 7 Z. G. Xia, Y. Y. Zhang, M. S. Molokeev and V. V. Atuchin, *J Phys Chem C*, 2013, 117, 20847.
- 8 Z. G. Xia, R. S. Liu, K. W. Huang and V. Drozd, *J. Mater. Chem.*, 2012, 22, 15183.
- 9 Wei Lv, Yongchao Jia, Wenzhen Lv, Qi Zhao and Hongpeng You, *New J.*

- Chem.*, 2014, DOI: 10.1039/c4nj00314d
- 10 Chien-Hao Huang, Wei-Ren Liu, Ting-Shan Chan and Yuan-Tai Lai, *Dalton Trans.*, 2014, 43, 7917
- 11 C. T. Chen, B. C. Wu, A. D. Jiang and G. You, *Sci. Sin. B*, 1985, 18, 235.
- 12 C. T. Chen, Y. C. Wu, A. D. Jiang, B. C. Wu, G. M. You, R. K. Li and S. J. Lin, *J. Opt. Soc. Am. B*, 1989, 6, 616.
- 13 L. Wu, X. L. Chen, H. Li, M. He, L. Dai, X. Z. Li and Y. P. Xu, *J. Solid State Chem.*, 2004, 177, 1111.
- 14 P. L. Li, Z. J. Wang, Z. P. Yang, Q. L. Guo and G. S. Fu, *Mater. Res. Bull.*, 2009, 44, 2068.
- 15 L. Wu, X. L. Chen, H. Li, M. He, Y. P. Xu and X. Z. Li, *Inorg. Chem.*, 2005, 44, 6409.
- 16 R. Norrestam, *Z. Kristallogr.*, 1989, 187, 1.
- 17 L. Wu, X. L. Chen, X. Z. Li, L. Dai, Y. P. Xu and M. Zhao, *Acta Crystallogr. C*, 2005, 61, i32.
- 18 N. G. Kononova, A. E. Kokh, T. B. Bekker, Furmanova N G, B. A. Maksimov, V. N. Molchanov and P. P. Fedorov, *Crystallogr. Rep.*, 2003, 48, 1114.
- 19 C. F. Guo, J. Yu, X. Ding, M. Li, Z. Y. Ren and J. T. Bai, *J. Electrochem. Soc.*, 2011, 158, J42.
- 20 S. S. Pitale, I. M. Nagpure, V. Kumar, O. M. Ntwaeaborwa, J. J. Terblans and H. C. Swart, *Mater. Res. Bull.*, 2011, 46, 987.
- 21 X. G. Zhang and M. L. Gong, *Dalton Trans.*, 2014, 43, 2465.
- 22 X. G. Zhang, J. H. Song, C. Y. Zhou, L. Y. Zhou and M. L. Gong, *J Lumin.*, 2014, 149, 69.
- 23 J. F. Sun, Z. P. Lian, G. Q. Shen and D. Z. Shen, *RSC Adv.*, 2013, 3, 18395.
- 24 A. K. Bedyal, V. Kumar, O. M. Ntwaeaborwa and H. C. Swart, *Mater. Res. Express*, 2014, 1, 015006.
- 25 W. R. Liu, C. H. Huang, C. P. Wu, Y. C. Chiu, Y. T. Yeh and T. M. Chen, *J. Mater. Chem.*, 2011, 21, 6869.
- 26 P. A. Nagpure and S. K. Omanwar, *J. Rare Earths*, 2012, 30, 856.
- 27 V. Kumar, A. K. Bedyal, S. S. Pitale, O. M. Ntwaeaborwa and H. C. Swart, *J. Alloys Compd.*, 2013, 554, 214.
- 28 X. G. Zhang, L. Y. Zhou and M. L. Gong, *ECS J. Solid State Sci. Technol.*, 2013, 2, R83.
- 29 S. Das, A. A. Reddy and G. V. Prakash, *Chemical Physics Letters*, 2011, 504, 206.
- 30 S. Das, A. A. Reddy, S. S. Babu and G. V. Prakash, *J. Mater. Sci.*, 2011, 46, 7770.
- 31 W. D. Cheng, H. Zhang, Q. S. Lin, F. K. Zheng and J. T. Chen, *Chem. Mater.*, 2001, 13, 1841.
- 32 Norrestam R., *Z. Kristallogr.*, 1989, 187, 103.
- 33 A. C. Larson and R. B. Von Dreele, in *LAUR*, 1994, pp. 86-748.
- 34 J. M. Tu and D. A. Keszler, *Acta Cryst.*, 1995, C51, 1962.
- 35 N. G. Kononova, A. E. Kokh, T. B. Bekker, N. G. Furmanova, B. A. Maksimov, V. N. Molchanov and P. P. Fedorov, *Crystallogr. Rep.*, 2003, 48, 1044.
- 36 G. Blasse and B. C. Grabmaier, *Lumin. Mater.*, 1994, 45.
- 37 J. W. H. van Krevel, H. T. Hintzen, R. Metselaar and A. Meijerink, *J. Alloys Compd.*, 1998, 268, 272.
- 38 D. L. Dexter, *J. Chem. Phys.*, 1953, 21, 836.
- 39 D. Wang, Q. R. Yin, Y. X. Li and M. Q. Wang, *J Lumin*, 2002, 97, 1.
- 40 Y. C. Chiu, W. R. Liu, C. K. Chang, C. C. Liao, Y. T. Yeh, S. M. Jang and T. M. Chen, *J. Mater. Chem.*, 2010, 20, 1755.
- 34 D. Haranath, H. Chander, P. Sharma and S. Singh, *Appl. Phys. Lett.*, 2006, 89, 173118.
- 42 A. Purwanto, W. N. Wang, T. Ogi, I. W. Lenggoro, E. Tanabe and K. Okuyama, *J. Alloys Compd.*, 2008, 463, 350.
- 43 J. S. Hou, X. Yin, Y. Z. Fang, F. Q. Huang and W. Z. Jiang, *Opt. Mater.*, 2012, 34, 1394.
- 44 Y. L. Huang, Y. Nakai, T. J. Tsuboi and H. J. Seo, *Opt. Express*, 2011, 19, 6303.